THERMAL ANALYSIS OF ALSEP PROTOTYPE "A"
CENTRAL STATION WITH COMPARISON TO TEST RESULTS

Prepared by _L. Hearin_

Approved by _J. L. McNaughton_

TABLE OF CONTENTS

ILLUSTRATIONS

TABLES

ALSEP CENTRAL STATION THERMAL ANALYSIS

1.0   Introduction

This document describes the analytical thermal model which was developed to determine the steady state temperature distribution of the prototype ALSEP Central Station in a lunar environment. Some test results are presented and compared with predictions made using the described model after preliminary correlation.

Section 2 describes the analytical model including the finite difference technique employed and the specific values of the parameters involved for the analytical model. Section 3 very briefly describes the computer program used to solve the finite difference network. This is followed by a comparison of the Prototype A test data with the analytical predictions both for the lunar noon and lunar night steady state conditions and a statement of the test conditions. Section 4 summarizes the conclusions drawn from the analysis and correlation.

1.1   Design Evolution

The fundamental ground rule governing the Central Station thermal control system design has been that it be a passive system. The system is designed to achieve isolation of the internal electronic components from the effects of the widely varying lunar thermal environment concomitant with maintenance of necessary radiation coupling to the space sink in order to achieve proper package thermal balance. Although thermal coatings with specified optical properties are employed the system is designed to function even if the optical properties of coatings exposed to direct solar radiation should be degraded by lunar dust. The primary effort in the design has been directed toward achieving isolation from the lunar environment and most of the specific design features are related to this.

The general configuration of the ALSEP Central Station thermal control system is shown in Figures 1 and 2. The salient features of the system are listed below. To better understand the objectives of the design it may be helpful to consider the radiator plate as the basic element in the

SUNSHIELD

MULTILAYER INSULATION

REFLECTOR

EXTENDER

RADIATOR PLATE

RADIATOR PLATE INSULATION

THERMAL PLATE ISOLATOR
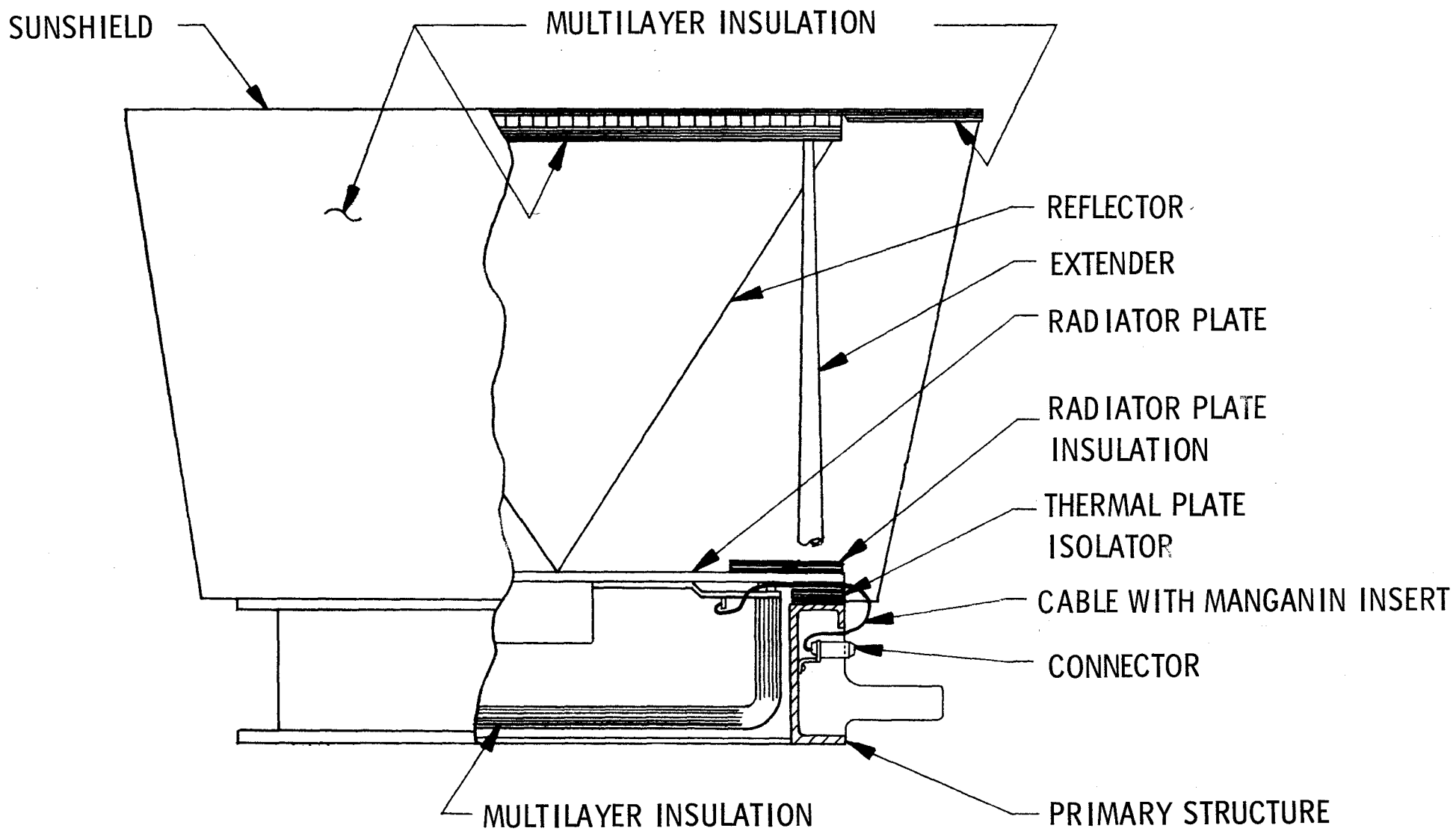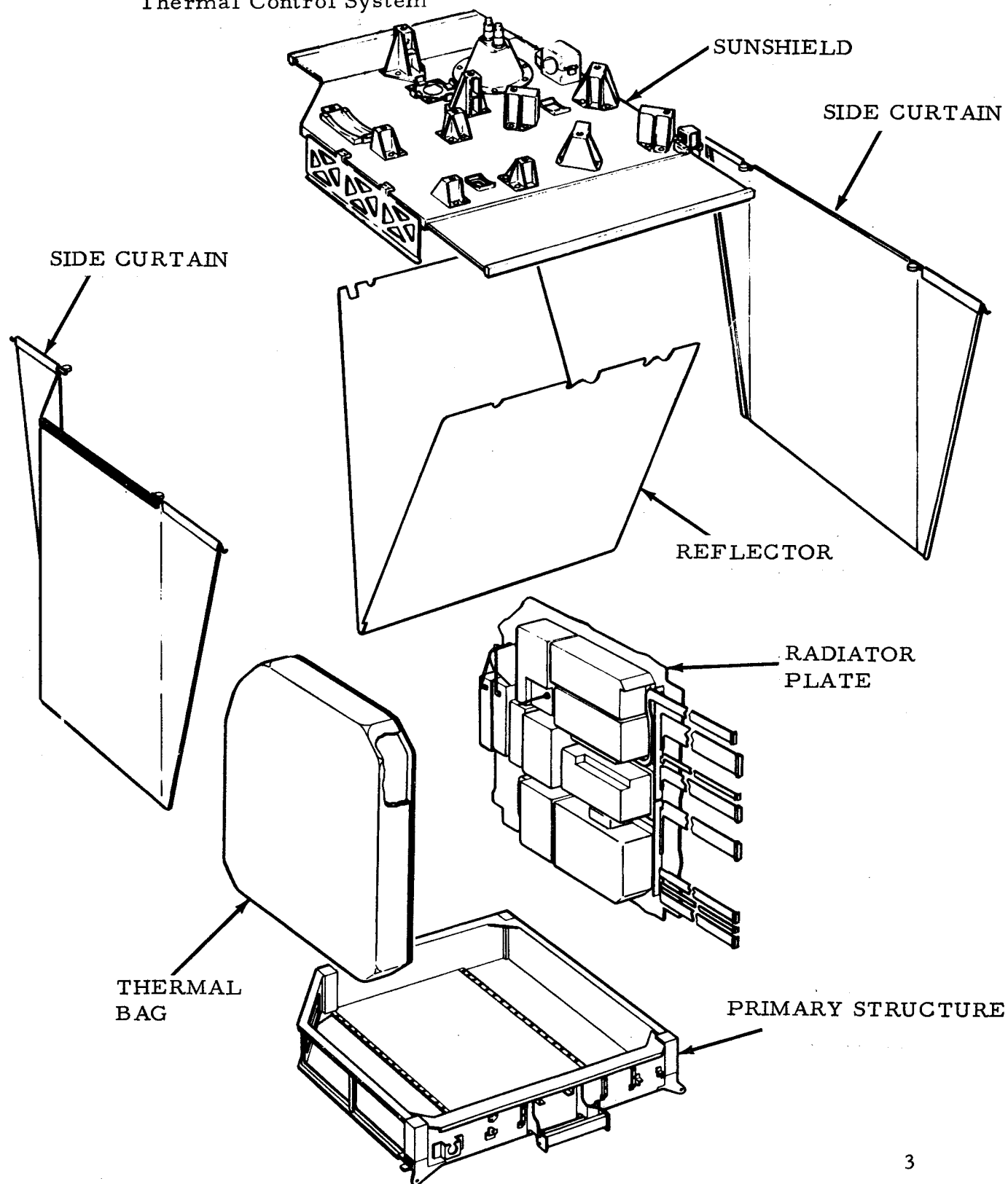
CABLE WITH MANGANIN INSERT

CONNECTOR

MULTILAYER INSULATION

PRIMARY STRUCTURE

Figure 1 Central Station Assembly

Figure 2 Primary Components of Central Station
Thermal Control System

SUNSHIELD

SIDE CURTAIN

SIDE CURTAIN

REFLECTOR

RADIATOR PLATE

THERMAL BAG

PRIMARY STRUCTURE

3

system (the radiator plate alone provides the means of regulating the effects of the internal heating) and all other features as accessory to the radiator (in that they provide isolation of the radiator plate from the lunar environment allowing it to properly carry out its function).

1. Radiator Plate. This is the "heart" of the system in that it provides the route by which the internal heating may be dissipated to deep space. With proper isolation from the lunar thermal environment and with given internal heating, the radiator plate configuration (radiation area, optical properties, etc.) is the essential determinant of the temperatures of the internal electronic components. The effective radiating area of the plate in the prototype design is approximately two square feet. This area is fixed by the size of the insulation which overlies the radiator and permits essentially no radiation heat flow from the radiator in the area it covers. The radiator is coated with white paint having a solar absorptivity, α, of approximately 0.2 and an infrared emissivity, ϵ, of approximately 0.9. This high emissivity provides a near maximum dissipation of internal heating per unit area of the radiator and results in a relatively small radiating area; this small radiating area contributes to better isolation of the radiator plate from the lunar surface. Approximately thirty to forty watts of internal heating are dissipated through this plate in the normal operational mode.

2. Insulation Bag. The multilayer insulation bag provides the major radiative isolation of the central station electronic components from the lunar thermal environment. It shields the electronic components from both direct solar radiation impingement as well as the infrared emission of the lunar surface itself, and in general provides a protective housing for the electronic components. It consists of alternate layers of aluminized mylar and glass fiber separators (approximately forty of each).

3. Sunshield. The primary function of the sunshield assembly (which for present purposes shall be considered to consist of the horizontal sunshield proper, as well as the side curtains) is to prevent direct solar heating of the radiator plate. With no sunshield and a degraded radiator surface the radiator temperature would rise well beyond acceptable limits during the

4

lunar day. The sunshield proper consists of an aluminum honey-comb structure coated on its exterior surface with white paint $(\alpha/\epsilon \approx 0.2/0.9)$ and insulated on its interior or underside surface with layers of crinkled aluminized mylar. The side curtains consist of alternate layers of aluminized mylar and a silk separators. The exterior aluminized mylar surface of the side curtains is overcoated with silicon monoxide, S_iO, $(\alpha/\epsilon \approx .15/.5)$. The sunshield assembly which is affixed to the primary central station structure with helical extenders is erected by the astronaut at the lunar deployment site. The sunshield proper also serves a secondary purpose by acting as a mounting pallet for ALSEP experiments during the lunar transit phase of the mission.

4. Reflector. In order to minimize radiative energy interchange between the radiator plate and the moon via the sunshield assembly a specular reflector has been provided. Originally this feature was not a part of the design. As the overall ALSEP design evolved, however, it became necessary to increase the sunshield height; the resulting size increase of the sunshield assembly resulted in a higher degree of indirect energy interchange between the radiator and the lunar surface. After considering several methods of reducing this detrimental effect, the present planar, automatically erecting reflector concept was selected. Tests were conducted to arrive at an optimum reflector configuration (consistent with packaging, deployment, reliability, manufacturing considerations etc.) and this configuration was incorporated into the design. The optimized reflector consists of a foldable aluminized mylar sheet which is attached to the sunshield and the radiator and which deploys automatically when the sunshield is erected. A $20^\circ F$ improvement (reduction) in temperature swing was realized with this reflector concept, as compared to the nonreflector configuration.

5. Radiator Plate Isolators. The radiator plate is solidly supported by the primary structure during the transit portion of the ALSEP mission. Since the primary structure rests directly upon the lunar surface during the operational mode, thermal isolation was required to minimize conduction between the radiator and the primary structure. The isolation concept selected consists of four spring-actuated standoffs which provide relatively long,

low conductivity conduction paths between the primary structure and the radiator. The concept is shown schematically in section in Figure 3. The standoff post is of fiberglas with a conductivity of approximately 0.2 Btu-ft/hr-ft^2-^{o}F. The spring material is stainless steel. The approximate total heat leak through these standoffs is 0.3 watts during the lunar night and less than .1 watts during the lunar day.

6. Cable Inserts. It was established early in the ALSEP design that cabling entering the insulated electronics compartment from the various remote experiments, the RTG power supply, etc. could be a major source of conduction. It was clear that if a section of low conductivity material could be inserted in the cabling at the point where it entered the insulated compartment the heat leakage could be reduced by approximately the ratio of the respective conductivities. Accordingly, a study of various materials was undertaken to find an optimum insert material. After consideration of several materials on the basis of electrical properties, magnetic properties, ease of joining, etc., as well as thermal conductivity, manganin was selected as the best all around material. A section of manganin wire was inserted in most of the cabling penetrating the central station electronics compartment. In general a typical manganin section extends from the external connector on the primary structure to the terminal board attached to the radiator plate see Figure 4 (a high resistance exists between the terminal board and the radiator plate). From test and analysis the maximum total heat leak through the cabling has been found to be approximately 3.5 watts for the lunar night and less than 1.0 watts for the lunar day.

Later sections of this report review the thermal analysis of each feature of the design and summarize the effect of each on the total system performance.

2.0   Basic Analytical Approach and Thermal Model

The analysis employs a finite difference approach wherein the physical configuration is subdivided into discreet, finite elements each of which is assumed to be isothermal. For purposes of analysis the mass of each element is assumed to be concentrated as its geometric center and

6

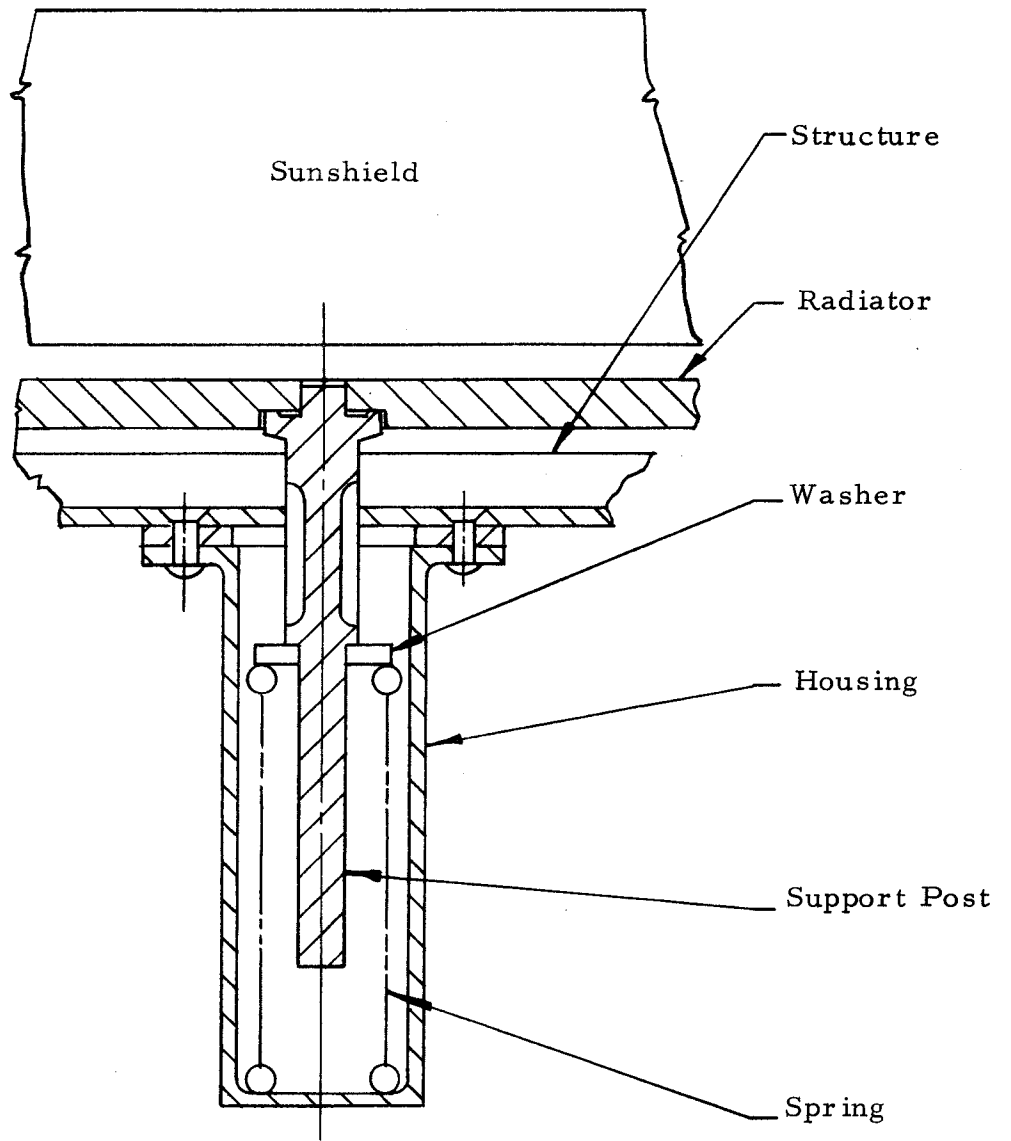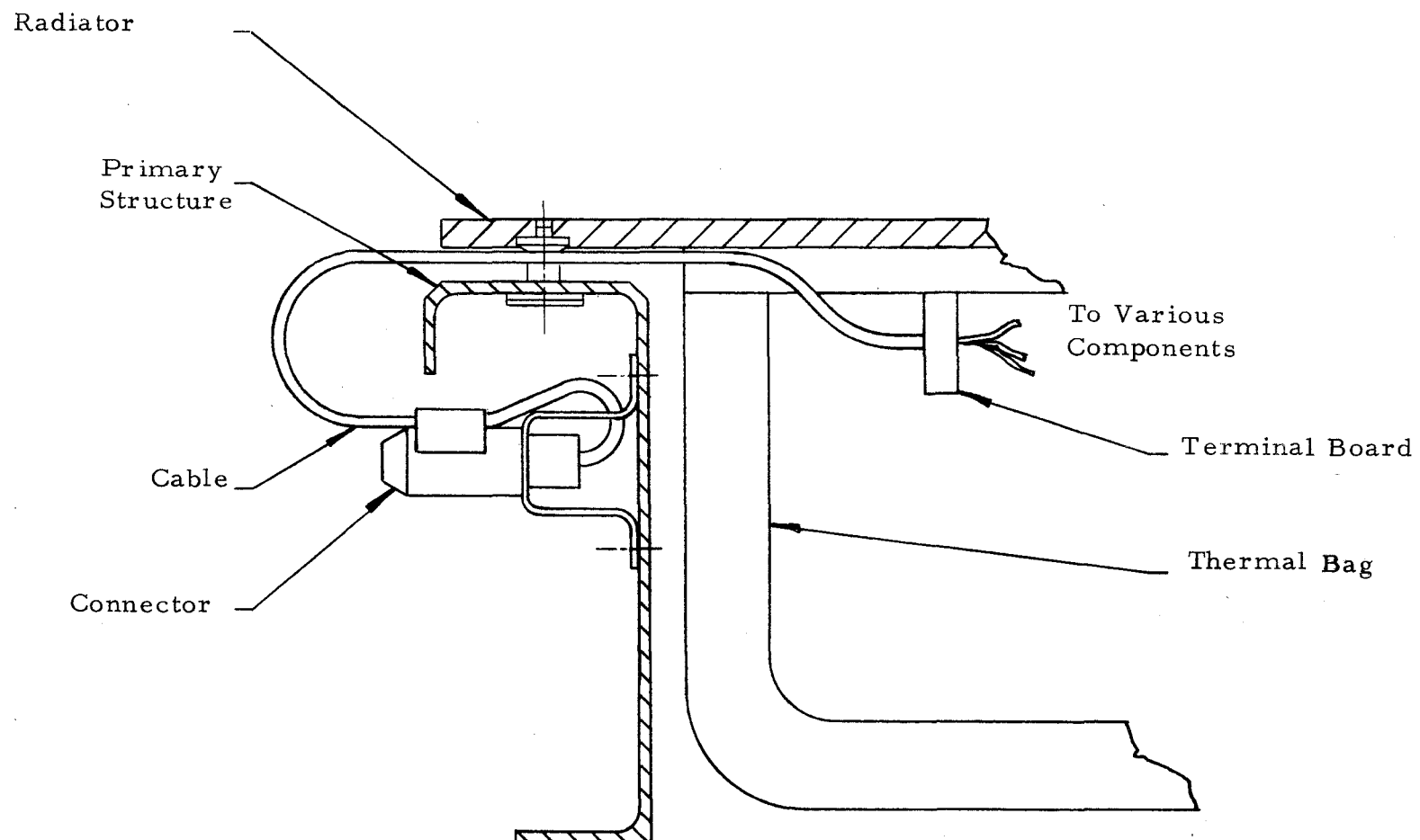Figure 3 Radiator Support Mechanism
(Stowed Configuration)

Radiator

Primary
Structure

Cable

Connector

To Various
Components

Terminal Board

Thermal Bag

NOTE: Manganin inserts extend from connector to terminal board.

Figure 4 Typical Cable Feed-Through

is termed a node. These nodes including their respective arbitrary heating are joined together in a resistance network, analogous to an electric circuit where temperature is analogous to voltage and heat flow is analogous to current. The nodal identification system is given below and determination of network parameters is given in the appropriate sections.

2.1 Node Identification

The node identification and numbering system are shown in Figures 5 to 11. Not shown are nodes 1 through 26 which are dummy nodes. These are radiosity nodes associated with nodes 101 through 126 respectively; they are a necessary part of the network but their temperatures in themselves have no significance in the analytical results. Nodes 27 through 33 represent exterior side curtain and sunshield nodes, 34 is the interior sunshield node, 35 and 36 are backside reflector nodes, nodes 37-48 represent electronic components, 49-53 the primary structure, 54 and 55 the insulation bag, 99 and 100 the noon and space respectively. Nodes 101-114 represent the radiator plate, 115 and 116 the radiator insulation, 117 and 118 the specular reflectors, 119-126 the interior side curtains and awning surfaces.

2.2 Radiation

The primary concern of this analysis from a radiation standpoint is the enclosure formed by the radiator, reflector, interior side curtain surfaces, the moon and space. Proper analysis of this enclosure is vital to validity of the thermal model since the radiation characteristics of this enclosure are the primary determinants of the thermal performance of the Central Station.

In order to account for all interreflections in this enclosure the Oppenheim radiosity network is employed. This technique is well documented (ref. 1) and the essentials of the approach are outlined in the Appendix of this report. As stated above, temperature is the driving potential in the network; this potential causes heat flow between nodes at a rate which is a function of the resistance between nodes. Thus determination of these resistance values is an essential part of the analysis. In general two types of resistors are required for the standard Oppenheim network, surface resistors and space resistors which are linked together with a dummy node or radiosity node. Each actual radiating node in the system is assumed to be at black body potential and is connected to a radiosity node through a surface resistance, which accounts for the non black properties

Sunshield Assembly

Reflector Assembly

Radiator-Baseplate
Insulation   Assembly

(Attached Electronic Components
Not Shown)

Insulation Bag
Assembly

Primary Structure
Assembly
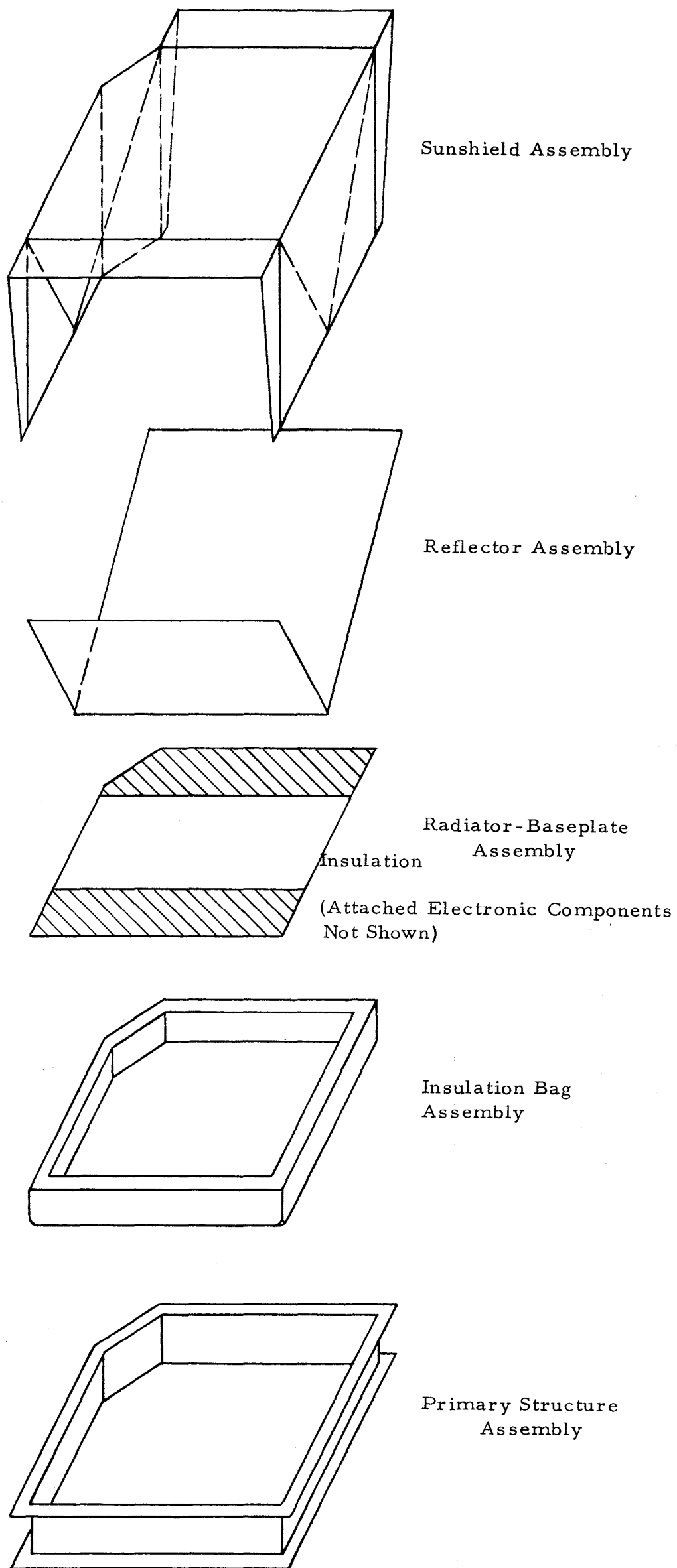
Figure 5 Exploded Schematic View of ALSEP Central
Station Thermal Control System
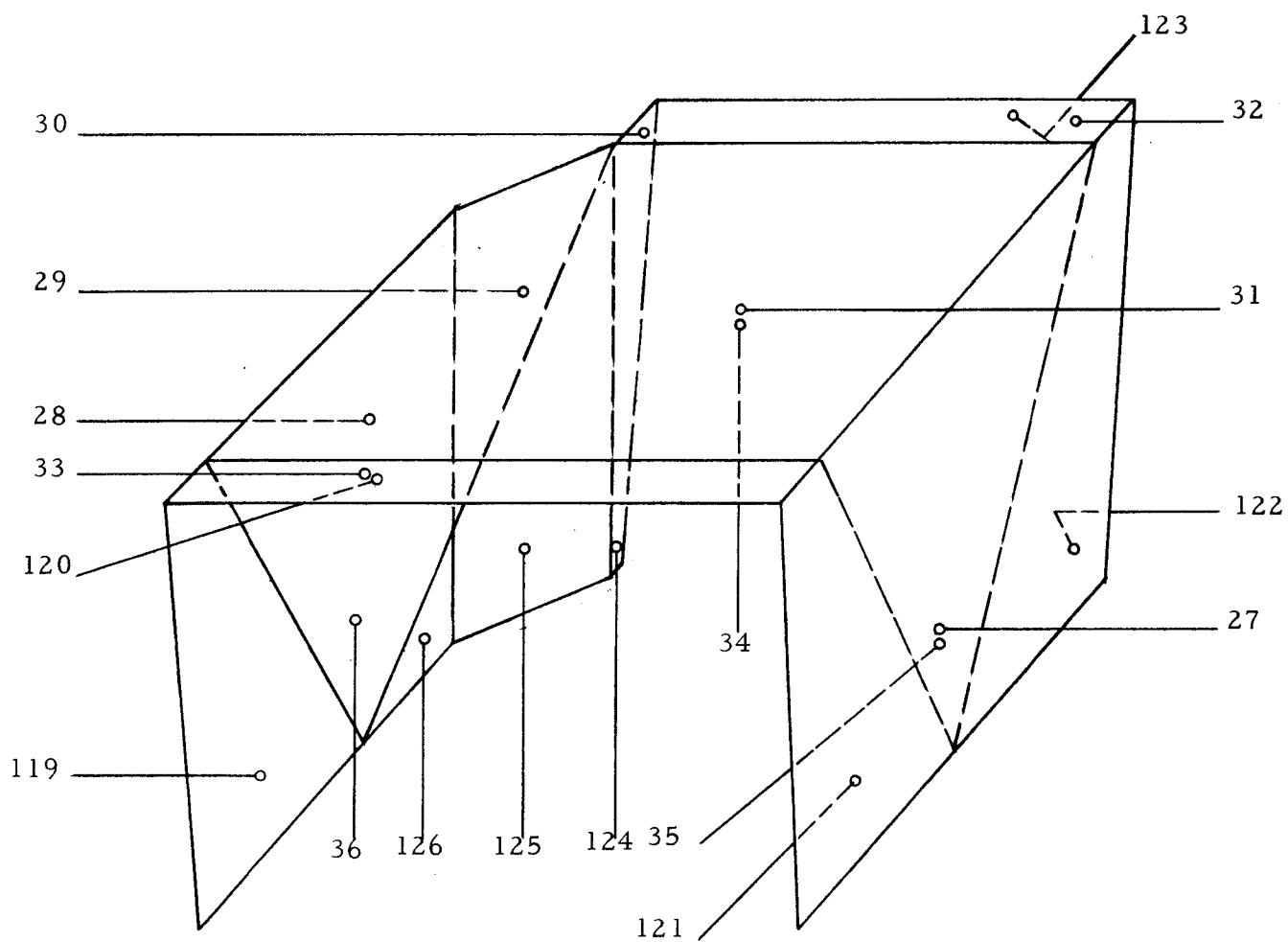
Figure 6 Sunshield Assembly Nodal Designation
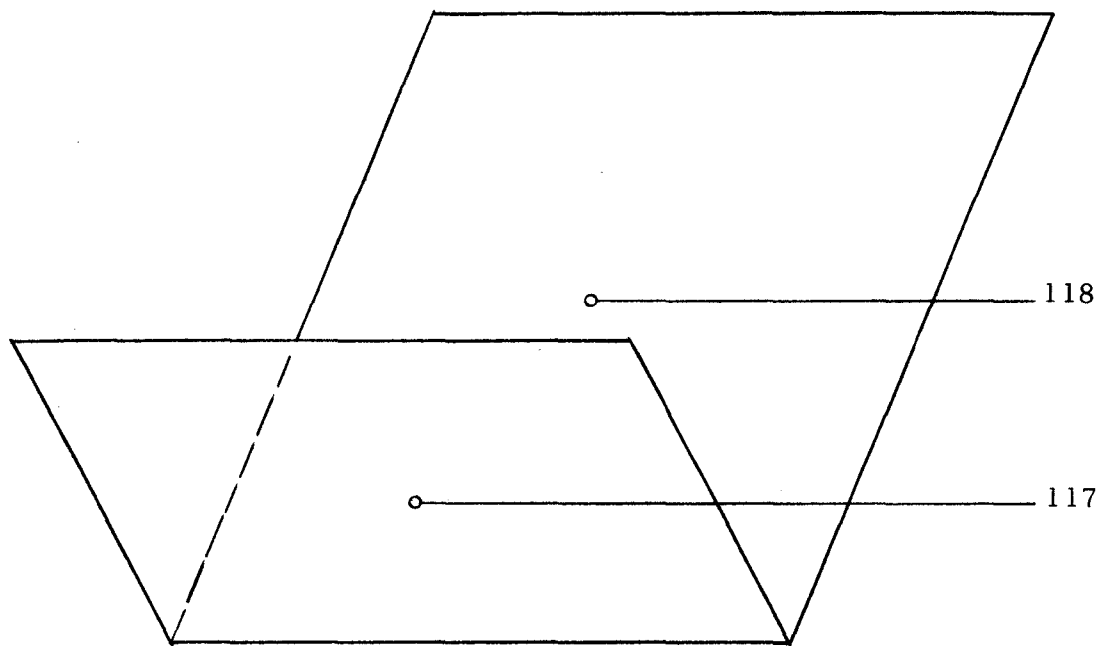
Figure 7 Reflector Assembly Nodal Designation
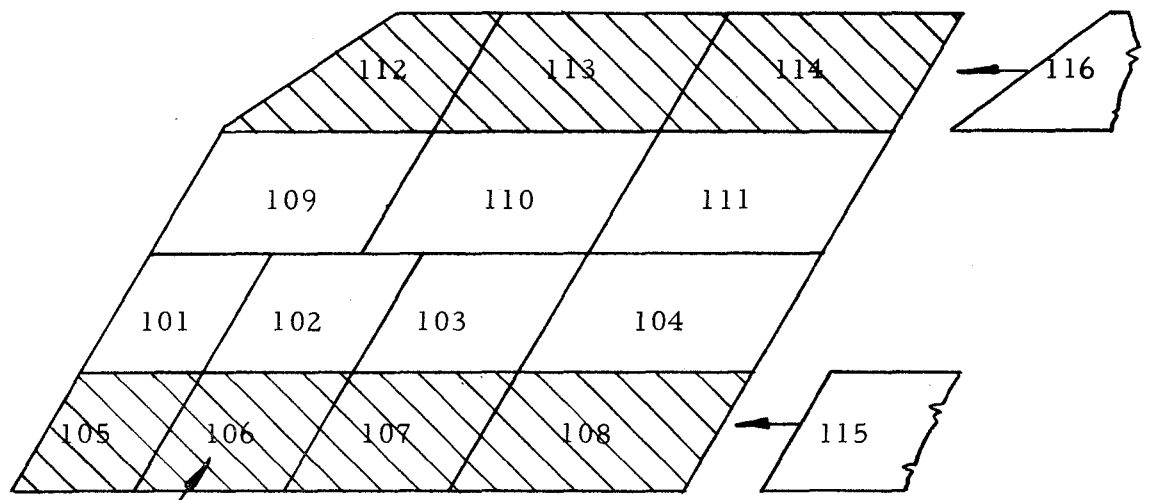
Indicates position of radiator insulation denoted by nodes 115 and 116. Attached electronic components identified on separate diagram.

Figure 8 Radiator-Baseplate Assembly Nodal Designation
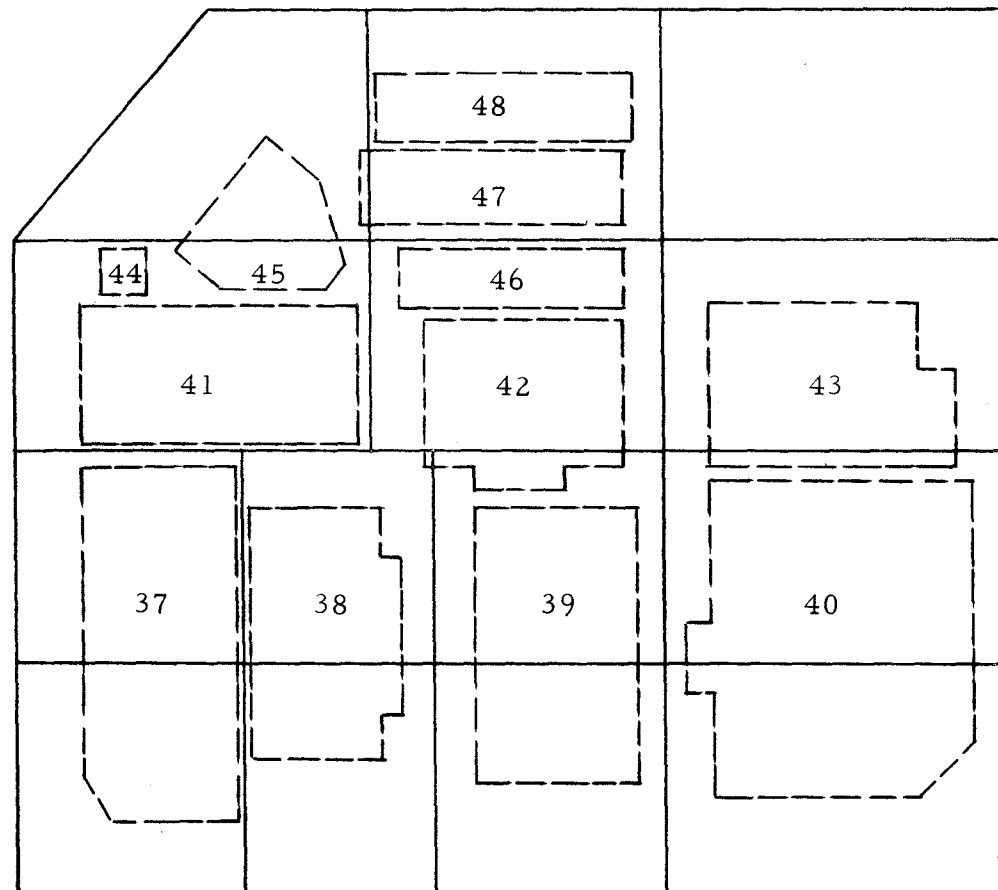
Top View

Figure 9 Radiator-Baseplate Assembly With Electronic
Components Identified

54 ~ Inner Fiberglass
Shell

55 ~ Outer Surface of Multilayer
Insulation Bag
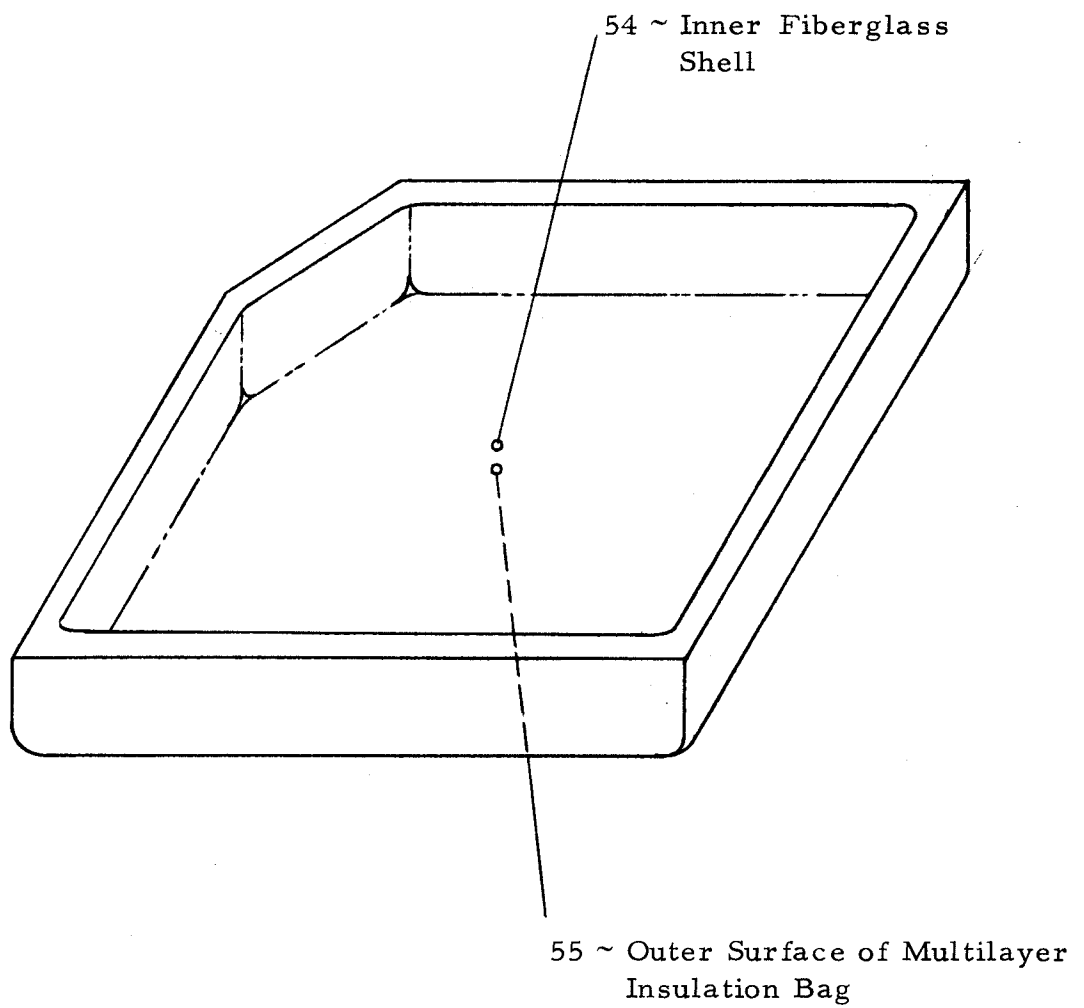
Figure 10 Insulation Bag Assembly Nodal Designation

53 ~ Aluminum Skin

51

50

52

49
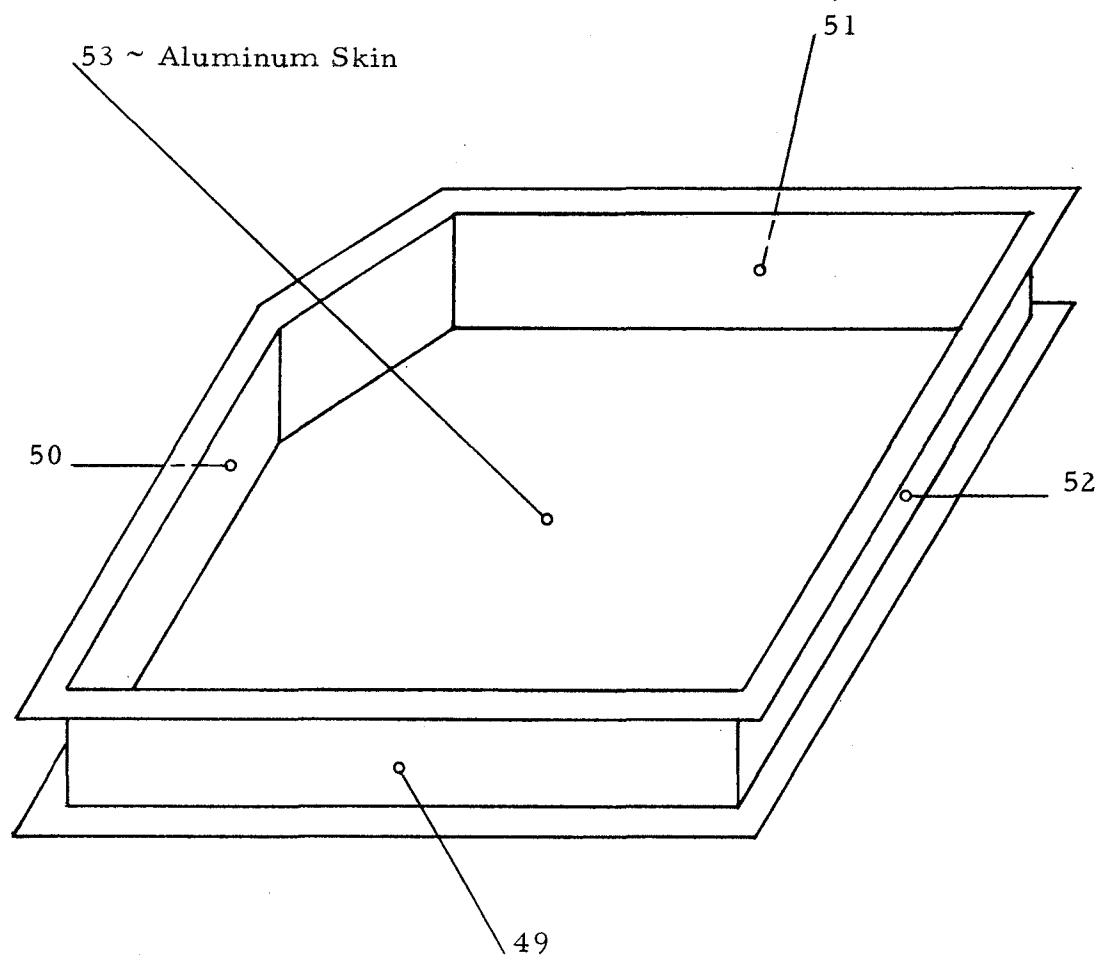
Figure 11 Primary Structure Assembly Nodal Designation

of the node; all radiosity nodes which "see" each other in the enclosure are then connected together by space resistors. The general form of the network is shown below for a two node system.

$$E_{b1} \quad \frac{1-\epsilon_1}{\epsilon_1 A_1} \quad J_1 \quad \frac{1}{A_1 F_{12}} \quad J_2 \quad \frac{1-\epsilon_2}{\epsilon_2 A_2} \quad E_{b2}$$

| Surface | Space | Surface |
| Resistance | Resistance | Resistance |

where:

E_b = black body emissive power of surface

J = diffuse flux density leaving surface (diffuse radiosity)

A = radiating area of surface

F = direct view factor between two surfaces

ϵ = emittance of surface.

subscripts:

1, 2 refer to surfaces 1 and 2 respectively.

When specular surfaces are present within the system the technique must be modified to take effects of specularity into account. The modification employed is based upon reference 2, wherein it is demonstrated how the Oppenheim approach for diffuse reflection may be applied to systems whose surfaces have a specular component to their reflectance. When one specular-diffuse surface is present in an enclosure of otherwise diffuse surfaces, four general types of resistors will exist in the radiosity network and will take the following general forms:

1)   Diffuse node surface resistance

$$E_{bm} \qquad\qquad J_m$$

$$R = \frac{1 - \epsilon_m}{A_m\, \epsilon_m}$$

2)   Specular-diffuse node surface resistance

$$E_{bi} \qquad\qquad E_{bi}$$

$$R = \frac{\rho_{d_i}}{A_i\, \epsilon_i\, (1 - \rho_{s_i})}$$

3)   Space resistance connecting diffuse nodes

$$J_m \qquad\qquad J_n$$

$$R = \frac{1}{A_m\, (F_{mn} + \rho_{s_i}\, F_{mn(i)})}$$

4) Space resistance connecting diffuse node with specular-diffuse
    node

$$J_m \qquad\qquad\qquad \frac{E_{bi}}{1 - \rho_{s_i}}$$

$$R = \frac{1}{(1 - \rho_{s_i}) A_m F_{mi}}$$

where:

A_j = radiating area of surface j

E_{bj} = black body emissive power of surface j

F_{jk} = direct view factor between surfaces j and k

$F_{jk(i)}$ = view factor between surfaces j and k as seen in the specular surface i

J_j = diffuse flux density leaving surface j (diffuse radiosity).

ϵ_j = emittance of surface j

ρ_{d_j} = diffuse reflectance of surface j

ρ_{s_j} = specular reflectance of surface j

The information required to utilize this method are 1) surface prop-
erties of each element of the network 2) view factors for each element
3) area of each element. Item 1 is specified in the design, and item 3 is
readily determined for the finite element network which has been con-
structed as shown previously. Item 2, the view factor determination is
more complicated for this case. It is rendered more difficult than usual

calculations of this type by the specular surface since now in addition to the direct geometric view factors, views "seen" through the specular surface must be accounted for. A combination of two approaches was used to evaluate the view factors. For the view factor relationship of elements within the reflector-radiator-sunshield enclosure Reference 3 was employed. Reference 3 is a program that permits direct evaluation of the radiation conductance (reciprocal of resistance), including specular effects, between surfaces of an enclosure consisting of plane polygons of any shape and orientation without a separate view factor calculation. Surfaces that can be represented as perfectly diffuse, perfectly specular or with both specular and diffuse components may be analyzed; the only program input required is the geometry and surface properties of the enclosure. The output includes the reciprocal of the space resistors as described above for direct use in the network. For configuration factors between elements of the radiator-reflector enclosure and the moon and space, Reference 3 is not applicable. For these cases Reference 4 was employed. Reference 4 is a generalized widely used computer program for determining view factors when the geometry of receiving and emitting surfaces are specified. When a specular surface is present not only must the actual geometry be specified but in addition the images of all surfaces as "seen" in the specular surface must be constructed and the view factors to each of them determined. The direct and specular views are then combined as described above in the modified Oppenheim network to yield the space resistor. It should be noted that the radiator reflector enclosure is separated into two independent parts each having one specular surface. These two enclosures are analyzed separately to determine the necessary radiation resistors and the results were combined into the complete radiosity network. In Figure 12 are shown schematically the two enclosures including the image surfaces as "seen" in the specular reflector surface.

For other portions of the model where the configuration is not precisely known, or where exact radiation analysis is impossible, impractical or relatively unimportant (such as the interior of the electronics compartment with its maze of wiring, electronic components etc.) radiation exchange between nodes is assumed to take the approximate form developed by Hottell (Ref. 5):

$$q_{1-2} = \sigma \, \epsilon_1 \, \epsilon_2 \, A_1 \, F_{1-2} \, (T_1^4 - T_2^4)$$
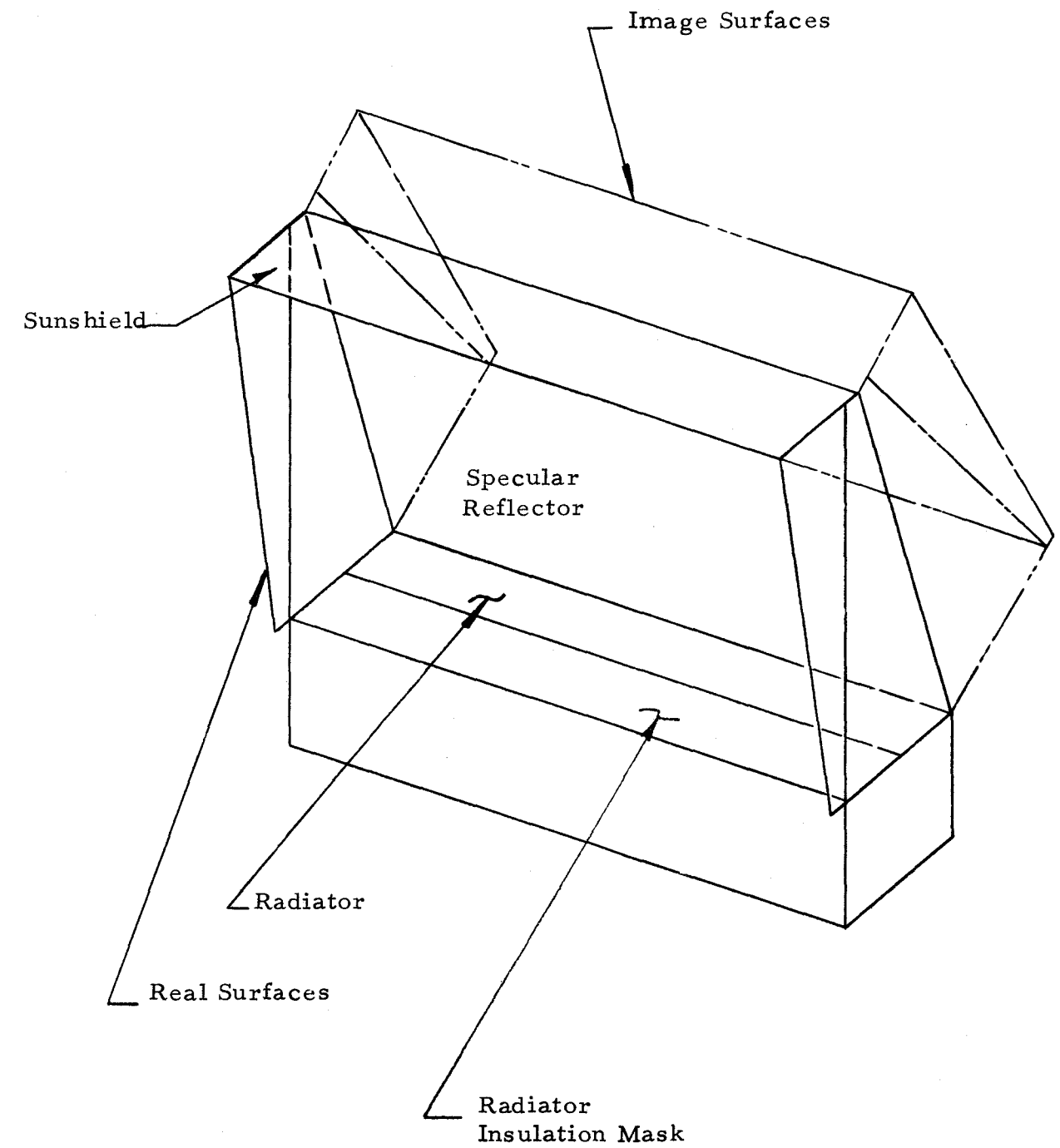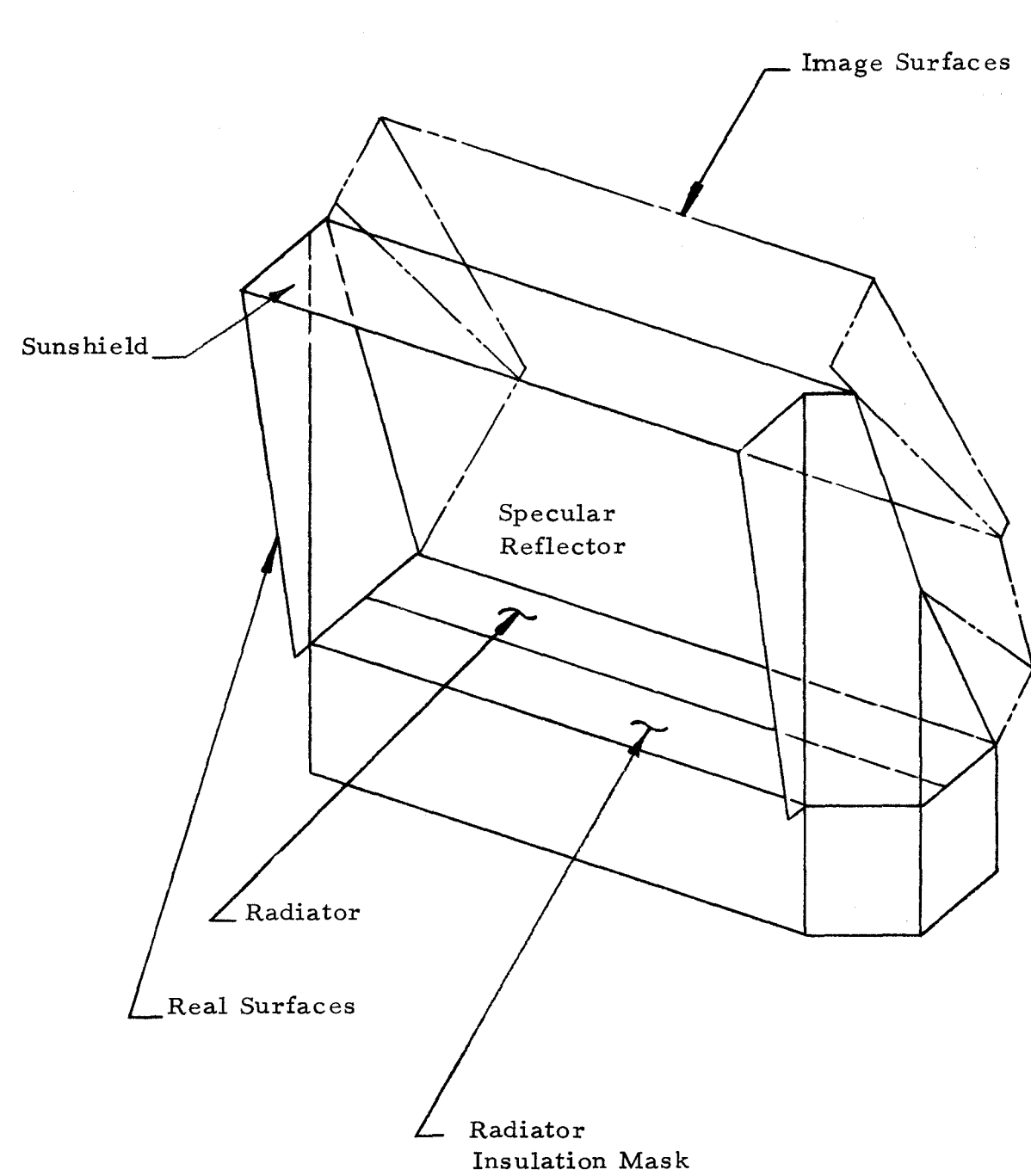
Figure 12 Typical Surface Image Construction

where q_{1-2} is the net heat exchange between nodes 1 and 2, T_1 and T_2 are the respective absolute temperatures, σ is the Stefan Boltzmann constant, and the other variables are as defined earlier. For this portion of the network, surface resistors are not employed and the radiation resistors are connected directly between the actual radiating nodes. The specific areas in which radiation is accounted for in this fashion are as follows:

1) Radiator to primary structure exterior. The horizontal flange of the structure is assumed to have a view factor of 1.0 to the radiator plate and an emittance of .01 to account for the multi-layer insulation on it.

2) Radiator to insulation bag interior. The interior of the insulation bag is assumed to have an infrared absorptance of 1.0 and the radiator plate interior an emissivity of 0.5 with a view factor to the bag of 0.5. The accuracy of these assumptions is not critical since in general the temperature of the bag and radiator are nearly equal.

3) Structure to insulation bag exterior.

4) Sunshield, side curtains, primary structure exterior to moon and space.

In Table 1 is a summary of the radiative properties of the surfaces in the system.

2.3 Conduction

Conduction heat transfer between nodes is assumed to take place according to the relation $q_{1-2} = \dfrac{T_1 - T_2}{R}$ where the conduction resistance R between 2 nodes is determined from the relation:

$$R = \frac{L_1}{K_1 A_1} + \frac{L_2}{K_2 A_2} + \frac{1}{h\,Ac}$$

TABLE 1

SUMMARY OF RADIATIVE PROPERTIES OF SURFACES IN
CENTRAL STATION THERMAL MODEL

	α	ϵ	Comments
Radiator Exterior	.2	.9	S13-G White Paint
Radiator Underside Seeing Primary Structure	NA	.05	Aluminized
Radiator Insulation	NA	.1	Aluminized Mylar
Specular Reflector	NA	.1	(Specular Reflectance = 0.9 (Diffuse Reflectance = 0.05
Side Curtain Exterior	.15	.5	SiO Over Aluminized Mylar
Side Curtain Interior	NA	.1	Aluminized Mylar
Sunshield Exterior	.2	.9	S13-G White Paint; Undegraded α
Sunshield Interior	NA	0.1	Aluminized Mylar
Primary Structure Exterior Except Bottom Skin	0.2	0.9	S13-G White Paint
Primary Structure Interior and Bottom Skin	NA	0.1	Aluminized
Insulation Bag - Exterior	NA	0.5	
Insulation Bag - Interior	NA	1.0	

L = distance from the center of one element to the interface of the elements between which conduction is taking place

K = thermal conductivity of the respective element

A = effective cross sectional area of the given element

h = interface conductance between elements

Ac = interface or contact area between elements

q = heat flux

T = temperature

1, 2 = subscripts representing the two respective elements.

The radiator plate is conductively isolated from the primary structure in the deployed configuration through spring loaded support posts as shown previously in Figure 3 (shown in stowed position). The total resistance through each post was computed and the appropriate radiator and primary structure nodes were joined with these resistors.

The cabling from the internal electronic components out of the insulation bag and to the connector on the primary structure is accounted for with conduction resistors. The total equivalent copper cross-section of wiring penetrating the insulated compartment is approximately 12000 circular mils. Of this, approximately 8000 circular mils is actually copper, with the remainder consisting of Manganin wire in amount equivalent to 4000 circular mils of copper. The equivalence is determined based upon the ratio of conductivity for copper and Manganin; the value used for copper is $240 \frac{Btu - ft}{hr - ft^2 - {}^{\circ}F}$ $15 \frac{Btu - ft}{hr - ft^2 - {}^{\circ}F}$ giving a ratio of approximately 16. The length of the Manganin insert is typically 8" in length. However since a portion of it is exposed to the lunar surface and to take into account possible radiation effects along the cable within the insulated compartment a value of 3" was used. Figure 4 schematically depicts the general arrangement of the cabling in relation to the insulated compartment.

Although a detailed thermal analysis of individual electronic components was not made, each component was considered in the overall central station thermal analysis in order to approximate the thermal gradients on the radiator plate. This was done by assuming each component (transmitter, PCU etc) as one node and attaching them with an interface area equal to that of the actual component and an interface conductance of 20 Btu/Hr-ft^2-$^{\circ}$F. This value of conductance is based upon the existance of silicon grease filler between the components and the thermal plate. The location of the components on the thermal plate was shown previously.

The multilayer insulation bag is assumed to consist of two nodes, the two exterior layers of the dexiglass-aluminized mylar composite. The resistance through the bag was computed using the bag thickness (distance between the two surface nodes) as the conduction length and average cross sectional area (parallel to the surface layers) as the conduction area. The thermal conductivity of the bag is $8.55*10^{-4} \frac{Btu - ft}{hr - ft^2 -^{\circ}F}$ for the day condition and $1.8*10^{-4} \frac{Btu - ft}{hr-ft^2 - ^{\circ}F}$ for the night condition (These values are based upon measured heat losses through an individual bag obtained during qualification testing by the bag subcontractor. The resistance values for the other multilayer insulation composites (side curtains, sunshield insulation, radiator insulation) were similarly determined.

The aluminum radiator plate is divided into fourteen nodes and the primary structure into 5 nodes as shown above. The resistance between these nodes is computed directly using the L/KA approach described earlier.

2.4 Heat Input

Two sources of arbitrary heating exist for the thermal model:

1) Internally generated heat of electronics

2) Solar radiation.

The internal heating of the electronic components is based on nominal lunar operation; the power is assumed constant throughout the lunar night and lunar day respectively. The component heating for lunar noon and lunar

night is listed in Table 2. The Lunar noon solar inputs are presented in Table 3. Solar heating values are determined from the following relation:

$$Q_{solar} = S \alpha A$$

where:

S = normal intensity of impinging solar radiation, $(442 \frac{Btu}{hr\text{-}ft^2}$ at lunar surface)

α = solar absorptance (fraction of impinging solar energy which is absorbed).

A = projected area of surface normal to impinging solar energy.

Solar heating of the lunar surface is accounted for by assuming all impinging solar energy is absorbed, and that emission occurs with $\epsilon_{moon} = 1.0$ (i. e. , lunar surface is a black body. In the case of the ALSEP Prototype "A" system test there was no solar heating and hence no albedo; in addition the simulated lunar surface is not a black body. These effects were accounted for in the analysis by correcting the lunar surface temperature to its effective black body value according to the following equation:

$$\sigma \, \epsilon_M \, T_M^4 = \sigma \, T_{eff}^4$$

where:

ϵ_M = emittance of simulated lunar surface

T_M = temperature of simulated lunar surface

T_{eff} = effective black body temperature of lunar surface.

3. 0   Thermal Analysis and Test Results

3. 1   Thermal Analysis Computer Program

With the analogous network parameters determined as described above it is necessary to solve the network for the steady state temperatures

26

TABLE 2

ELECTRONIC COMPONENT HEAT INPUT

Node No.	Description	Table No. (Computer Input)	Heat Input (Watts) Day	Night
37	PCU	4	16.7	17.0
38	PDU	5	1.8	1.8
39	Analog Multiplex Converter	6	1.4	1.4
40	Passive Seismic	7	4.4	4.4
41	Comm. Receiver	8	0.7	0.7
42	Data Processor	9	0.5	0.5
43	Comm. Decoder	10	1.3	1.3
44	Timer	--	0	0
45	Diplexer Switch	12	0	0.15
46	Diplexer Filter	--	0	0
47	Transmitter A	14	6.9	0
48	Transmitter B	14	0	5.9
--	Harness Loss	12	0.3	0.4
--	Dust Detector	12	0.6	0.2

TABLE 3

LUNAR NOON SOLAR HEAT INPUT

Node No.	Description	Table No. (Computer Input)	BTU/HR.
31	Sunshield	3	403.0
32	Awning	2	56.5
33	Awning	2	72.3

of each node in the system. At steady state the net heat flow at any node of the system must equal zero. Thus it is necessary to solve a set of simultaneous non-linear equations which describe the heat balance of each node of the system. This is achieved with the thermal analysis computer program described in Reference 6. The input required by this program for the solution of a steady state network are 1) temperature of each node, 2) conduction resistances in the network, 3) K for the radiation portion of the network where K is either $\epsilon_1 \epsilon_2 A_1 F_{12}$ or the reciprocal of the radiosity network resistance described above. The resistor input generated for the Prototype "A" test analysis described in this report is listed in Tables 4 and 5 for the radiation portion and Table 6 for the conduction portion.

3.2 Test Description

The details of the Prototype "A" test set up and conditions are presented elsewhere (ref 7 for example) and will only be commented on briefly here. The major objective of the Prototype "A" system test was to evaluate the ALSEP system thermal performance at steady state lunar noon and lunar night conditions. The test was carried out in the Bendix Aerospace Systems Division 20' x 27' thermal/vacuum chamber. The main portion of ALSEP (including the central station) was arranged in the chamber on a square lunar surface simulator approximately 14' x 14'. This simulator is maintained at 250°F during lunar noon simulation and at -300°F during lunar night simulation. The chamber shroud is maintained at -300°F for both lunar noon and lunar night conditions. Solar simulation for the Central Station is provided by an overhead array of infrared lamps. The IR lamps cause the sunshield to absorb the same total amount of radiant energy that would be absorbed under actual lunar conditions (solar heating) with the same sunshield surface properties. During these tests the ALSEP was functioning in a normal operation mode. This resulted in a total internal Central Station thermal dissipation of 34.6 watts and 33.6 watts for lunar noon and lunar night conditions respectively.

3.3 Comparison of Analysis and Test Results

In Table 7 are shown the central station steady state temperatures as predicted for the complete model of the Prototype "A" configuration under chamber conditions. Table 8 shows a comparison between predicted and measured results of the Prototype test (it should be noted that it was not possible to measure a temperature at each node of the previously constructed analytical model). Figures 13 and 14 depict this correlation for

TABLE 4

BASIC RADIATION RESISTOR INPUT FOR THAT PORTION OF NETWORK EMPLOYING HOTTELL EQUATION

Res. #	Nodes Conn.	$\epsilon_1 \epsilon_2 A_1 F_{12}$	Comments
57	105-49	$.178 \times 10^{-4}$	Radiator to structure
58	106-49	$.178 \times 10^{-4}$	
59	107-49	$.178 \times 10^{-4}$	
60	108-49	$.178 \times 10^{-4}$	
61	101-50	$.15 \times 10^{-4}$	
62	105-50	$.15 \times 10^{-4}$	
63	109-50	$.15 \times 10^{-4}$	
64	112-50	$.15 \times 10^{-4}$	
65	112-51	$.213 \times 10^{-4}$	
66	113-51	$.213 \times 10^{-4}$	
67	114-51	$.213 \times 10^{-4}$	
68	104-52	$.162 \times 10^{-4}$	
69	108-52	$.162 \times 10^{-4}$	
70	111-52	$.162 \times 10^{-4}$	
71	114-52	$.162 \times 10^{-4}$	
72	101-54	$.571 \times 10^{-1}$	Radiator to insulation bag
73	102-54	$.493 \times 10^{-1}$	
74	103-54	$.595 \times 10^{-1}$	
75	104-54	$.88 \times 10^{-1}$	
76	105-54	$.605 \times 10^{-1}$	
77	106-54	$.52 \times 10^{-1}$	
78	107-54	$.625 \times 10^{-1}$	
79	108-54	$.925 \times 10^{-1}$	
80	109-54	$.92 \times 10^{-1}$	
81	110-54	$.74 \times 10^{-1}$	
82	111-54	$.88 \times 10^{-1}$	
83	112-54	$.655 \times 10^{-1}$	
84	113-54	$.78 \times 10^{-1}$	
85	114-54	$.925 \times 10^{-1}$	
86	49-55	$.168 \times 10^{-1}$	Primary structure to insulation bag
87	50-55	$.169 \times 10^{-1}$	
88	51-55	$.128 \times 10^{-1}$	
89	52-55	$.153 \times 10^{-1}$	

TABLE 4 (Cont.)

BASIC RADIATION RESISTOR INPUT FOR THAT PORTION
OF NETWORK EMPLOYING HOTTELL EQUATION

Res. #	Nodes Conn.	$\epsilon_1 \epsilon_2 A_1 F_{1-2}$	Comments
90	53-55	$.1015 \times 10^{-1}$	Primary structure to insulation bag
96	49-99	.302	Structure to moon and space
97	49-100	.302	
98	50-99	.304	
99	50-100	.304	
100	51-99	.23	
101	51-100	.23	
102	52-99	.274	
103	52-100	.274	
285	53-99	.365	
122	27-99	1.33	
123	77-100	1.33	
124	28-99	1.19	
125	28-100	1.19	
126	29-99	.37	
127	29-100	.74	
128	30-99	.134	
129	30-100	.134	
131	31-100	3.74	
133	33-100	.55	
135	32-100	.426	
136	34-117		Reflector, sunshield, side curtain interior - Evaluated using Gebhart absorption factor technique
137	34-35		
138	34-118		
139	34-36		
140	117-35		
141	117-118		
142	117-36		
143	35-118		
144	35-36		
145	118-36		

TABLE 5

BASIC RADIATION RESISTOR INPUT FOR THAT PORTION OF THE
NETWORK EMPLOYING THE RADIOSITY METHOD

Res. #	Nodes Conn.	$\frac{1}{R}$	Comments
146	1-2	2.218×10^{-3}	Resistors 146-264 make up the
147	1-3	4.495^{-4}	network in the enclosure con-
148	1-4	1.401^{-4}	sisting of the radiator, re-
149	1-15	3.292^{-3}	flector, curtains, moon and
150	1-19	$.8079^{-1}$	space
151	1-17	2.464^{-2}	
152	1-21	1.448^{-2}	
153	1-20	1.810^{-2}	
*154	1-99	3.100^{-3}	
*155	1-100	$.7823^{-1}$	
156	2-3	1.675^{-3}	
157	2-4	3.001^{-4}	
158	2-15	3.800^{-3}	
159	2-16	4.095^{-2}	
160	2-17	2.431^{-2}	
161	2-21	1.903^{-2}	
162	2-20	1.740^{-2}	
*163	2-99	2.487^{-3}	
*164	2-100	$.8231^{-1}$	
165	3-4	2.685^{-3}	
166	3-15	4.904^{-3}	
167	3-19	3.006^{-2}	
168	3-17	2.966^{-2}	
169	3-21	3.573^{-2}	
170	3-20	2.148^{-2}	
*171	3-99	2.142^{-3}	
*172	3-100	1.062^{-1}	
173	4-15	5.709^{-3}	
174	4-19	2.469^{-2}	
175	4-17	2.300^{-2}	
176	4-21	1.086^{-1}	
177	4-20	2.901^{-2}	
*178	4-99	3.158^{-3}	

TABLE 5 (Cont.)

BASIC RADIATION RESISTOR INPUT FOR THAT PORTION OF THE NETWORK EMPLOYING THE RADIOSITY METHOD

Res. #	Nodes Conn.	$\dfrac{1}{R}$	Comments
*179	4-100	1.319^{-1}	Resistors 146-264 make up the
180	15-19	1.810^{-1}	network in the enclosure con-
181	15-17	1.068^{-1}	sisting of the radiator, re-
182	15-21	2.008^{-1}	flector, curtains, moon and
183	15-20	1.022×10^{-1}	space
*184	15-99	2.802^{-2}	
*185	15-100	4.676^{-1}	
186	19-17	1.149^{-1}	
187	19-21	2.475^{-1}	
188	19-20	1.556^{-1}	
*189	19-99	2.382^{-1}	
*190	19-100	4.939^{-1}	
191	17-21	1.150^{-1}	
192	17-20	5.207^{-2}	
*193	17-99	1.238^{-1}	
*194	17-100	1.349^{-1}	
195	21-20	2.078^{-1}	
*196	21-99	3.071^{-1}	
*197	21-100	4.221^{-1}	
*198	20-99	5.225^{-1}	
200	11-10	2.744^{-3}	
201	11-9	2.201^{-4}	
202	11-16	5.575^{-3}	
203	11-22	1.076^{-1}	
204	11-23	2.469^{-2}	
205	11-24	1.133^{-2}	
206	11-25	2.411^{-2}	
207	11-26	3.450^{-3}	
208	11-18	3.940^{-2}	
*209	11-99	$.7005^{-2}$	
*210	11-100	1.150^{-1}	
211	10-9	2.750^{-3}	
212	10-16	5.458^{-3}	

TABLE 5 (Cont.)

BASIC RADIATION RESISTOR INPUT FOR THAT PORTION OF THE NETWORK EMPLOYING THE RADIOSITY METHOD

Res. #	Nodes Conn.	$\frac{1}{R}$	Comments
213	10-22	4.180^{-2}	Resistors 146-264 make up the
214	10-23	2.154^{-2}	network in the enclosure con-
215	10-24	1.011^{-2}	sisting of the radiator, re-
216	10-25	4.582^{-2}	flector, curtains, moon and
217	10-26	$.8973^{-2}$	space
218	10-18	3.654^{-2}	
*219	10-99	5.073^{-3}	
*220	10-100	1.068^{-1}	
221	9-16	4.845^{-3}	
222	9-22	2.633^{-3}	
223	9-23	2.131^{-2}	
224	9-24	2.047^{-3}	
225	9-25	$.9467^{-1}$	
226	9-26	$.6205^{-1}$	
227	9-18	3.795^{-2}	
*228	9-99	4.308^{-3}	
*229	9-100	$.8523^{-1}$	
230	16-22	1.798^{-1}	
231	16-23	$.7472^{-1}$	
232	16-24	3.450^{-2}	
233	16-25	1.375^{-1}	
234	16-26	2.475^{-2}	
235	16-18	$.7525^{-1}$	
*236	16-99	2.312^{-2}	
*237	16-100	3.170^{-1}	
238	22-23	1.713^{-1}	
239	22-24	1.226^{-1}	
240	22-25	1.556^{-1}	
241	22-26	3.973^{-2}	
242	22-18	1.074^{-1}	
*243	22-99	3.076^{-1}	
*244	22-100	3.748^{-1}	
245	23-24	1.010^{-1}	

TABLE 5 (Cont.)

BASIC RADIATION RESISTOR INPUT FOR THAT PORTION OF THE NETWORK EMPLOYING THE RADIOSITY METHOD

Res. #	Nodes Conn.	$\dfrac{1}{R}$	Comments
246	23-25	3.912^{-2}	Resistors 146-264 make up the
247	23-26	$.8523^{-2}$	network in the enclosure con-
248	23-18	3.981^{-2}	sisting of the radiator, re-
*249	23-99	3.707^{-1}	flector, curtains, moon and
*250	23-100	1.080^{-1}	space
243	24-18	3.398^{-2}	
*254	24-99	$.9399^{-1}$	
*255	24-100	1.938^{-1}	
256	25-26	2.562^{-2}	
257	25-18	1.086^{-1}	
*259	25-100	1.395^{-1}	
260	26-18	1.565^{-2}	
*261	26-99	1.839^{-2}	
*262	26-100	4.530^{-2}	
*263	18-99	$.9224^{-1}$	
*264	18-100	1.027^{-1}	
266	1-101	2.072	Surface Resistor
267	2-102	1.781	
268	3-103	2.137	
269	4-104	3.158	
270	15-115	1.197^{-1}	
271	19-119	1.932^{-1}	
**272	17-117	5.073^{-1}	
273	21-121	1.932^{-1}	
274	20-120	1.389^{-1}	
275	11-111	3.158	
276	10-110	2.656	
277	9-109	3.322	
278	16-116	1.057^{-1}	
279	22-122	1.932^{-1}	
280	23-123	1.092^{-1}	
281	24-124	$.7239^{-1}$	
282	25-125	1.249^{-1}	
283	26-126	3.187^{-2}	
**284	18-118	4.518^{-1}	

*Evaluated using CONFAC II to determine individual view factors. Other resistors in this group determined directly using ref. 3.

**Specular surface involved.

TABLE 6

CONDUCTION RESISTOR INPUT

Resistor No.	Connecting Nodes	R	Comments
1	113-48	.48	Components to radiator
2	113-47	.48	
3	112-45	.99	
4	109-45	1.03	
5	110-46	4.62	
6	109-41	.224	
7	110-42	.385	
8	103-42	.8	
9	111-43	.362	
10	104-43	.916	
11	101-37	.218	
12	105-37	.6	
13	102-38	.357	
14	106-38	.68	
15	103-39	.483	
16	107-39	.252	
17	104-40	.252	
18	108-40	.369	
19	101-102	.875	Radiator node connections
20	101-105	.931	
21	101-109	.907	
22	102-103	.893	
23	102-106	1.085	
24	102-110	3.54	
25	102-109	1.5	
26	103-104	1.21	
27	103-107	.903	
28	103-110	.88	
29	104-108	.61	
30	104-111	.594	
31	105-115	8.6	
32	106-115	10.0	
33	107-115	8.32	

TABLE 6 (Cont.)

CONDUCTION RESISTOR INPUT

Resistor No.	Connecting Nodes	R	Comments
34	108-115	5.63	Radiator node connections
35	105-106	.833	
36	106-107	.848	
37	107-108	1.15	
38	111-111	1.33	
39	111-114	.61	
40	104-111	.595	
41	109-110	1.36	
42	110-113	.722	
43	102-110	3.54	
44	103-110	.88	
45	109-112	.58	
46	101-109	.907	
47	102-109	1.5	
48	112-116	7.95	Radiator to insulation mask
49	113-116	6.7	
50	114-116	5.63	
51	112-113	1.3	Radiator node connection
52	113-114	1.26	
53	105-49	1000.	Radiator to structure
54	109-49	1000.	Through spring supports
55	114-51	1000.	
56	113-51	1000.	
91	54-55	10.55 (day) 50.0 (night)	Insulation bag resistance
92	49-50	13.73	Structure node connections
93	50-51	12.8	
94	51-52	12.0	
95	52-49	10.9	
104	40-49	46.3	Cable resistors
105	37-49	37.4	
106	38-49	212.	
107	43-49	570.	
108	39-49	493.	
109	42-49	616.	

TABLE 6 (Cont.)

CONDUCTION RESISTOR INPUT

Resistor No.	Connecting Nodes	R	Comments
110	119-28	5.26	Side curtain
111	120-33	7.64	Awning
112	121-27	5.26	Side curtain
113	122-27	5.26	↓
114	123-32	9.78	Awning
115	124-30	15.5	Side curtain
116	125-29	8.0	
117	126-28	34.6	
118	27-35	39.4	
119	28-36	4.38	
120	29-36	20.8	
121	31-34	2.0	↓
265	44-109	4.6	Component to radiator
286	49-53	5.68	Structure connection
287	50-53	7.26	
288	51-53	5.81	↓
289	52-53	7.31	
290	53-99	33.3	Structure to moon

TABLE 7

PREDICTED TEMPERATURES FOR PROTOTYPE "A"
THERMAL VACUUM TEST

Node No.	Temperature (°F)		Node No.	Temperature (°F)	
	Lunar Noon	Lunar Night		Lunar Noon	Lunar Night
27	129	-264	103	115	-15
28	128	-268	104	113	-19
29	128	-257	105	132	1
30	128	-264	106	123	-7
31	46	-289	107	118	-13
32	79	-259	108	116	-17
33	82	-261	109	122	-9
34	62	-287	110	116	-15
35	103	-248	111	113	-20
36	119	-265	112	124	-8
37	140	8.0	113	126	-6
38	123	-8.4	114	117	-16
39	118	-13	115	54	-158
40	116	-16	116	68	-138
41	123	-8	117	105	-176
42	116	-14	118	105	-164
43	114	-18	119	111	-261
44	122	-9	120	139	-255
45	125	-7	121	118	-257
46	116	-15	122	120	-255
47	138	-6	123	123	-252
48	126	3	124	112	-259
49	140	-197	125	119	-244
50	139	-224	126	112	-247
51	143	-226			
52	140	-222			
53	193	-221			
54	122	-16			
55	161	-132			
99	241	-300			
100	-300	-300			
101	130	0			
102	120	-10			

TABLE 8

COMPARISON OF MEASURED AND PREDICTED CENTRAL
STATION TEMPERATURES DURING PROTOTYPE "A" T/V TEST

Sensor ID	Analysis Node No.	Temperature (°F)				Description
		Lunar Noon		Lunar Night		
		Pred.	Meas.	Pred.	Meas.	
CS1	31	46	40	-289	-232	Sunshield
CS2	31	46	42	-289	-230	↓
CS3	31	46	41	-289	-230	
CS4	101	130	114	0	-5	Radiator
CS5	113	126	106	-6	-15	
CS6	113	126	105	-6	-14	
CS7	114	117	100	-16	-22	
CS8	109	122	107	-9	-13	
CS9	105, 106	127	109	-3	-11	
CS10	107	118	103	-13	-18	
CS11	101, 102, 109	124	106	-6	-13	
CS12	103, 110	115	102	-15	-17	
CS13	104, 111	113	98	-20	-22	
CS14	114	117	102	-16	-18	↓
CS22	52	140	165	-222	-157	Primary Structure
CS23	51	143	179	-226	-159	↓
CS24	50	139	185	-224	-142	
CS25	53	193	232	-221	-144	Primary Structure Bottom Skin

Figure 13 ALSEP Prototype "A" System Test; Measured vs Predicted
Radiator Temperatures For Lunar Noon (^{O}F)

xxx = Measured
(xxx) = Predicted

-14
(-6)

-22
(-16)

-15
(-6)

-13
(-9)
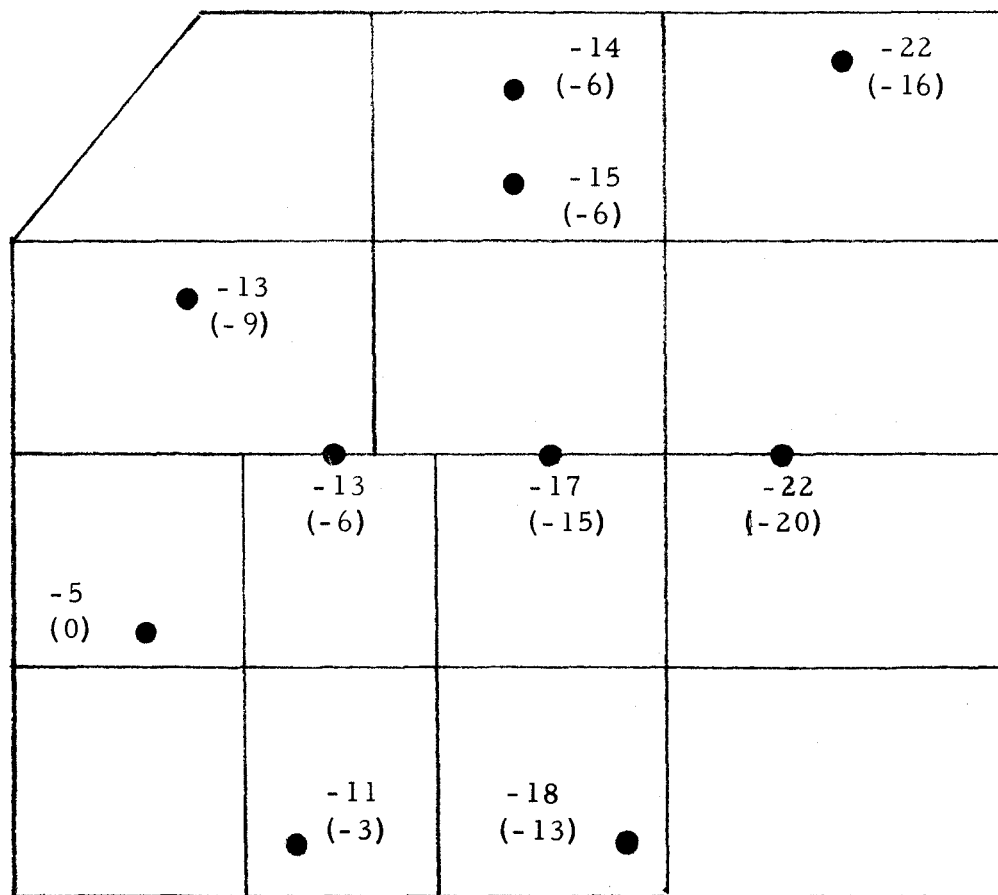
$T_{Ave_{Meas}} = -15$

$T_{Ave_{Pred}} = -11$

(14 nodes)

-13
(-6)

-17
(-15)

-22
(-20)

-5
(0)

-11
(-3)

-18
(-13)

Figure 14   ALSEP Prototype "A" System Test; Measured vs Predicted
Radiator Temperatures For Lunar Night (^{O}F)

the radiator plate, the most critical element of the central station from a thermal control standpoint. Figure 15 is a heat balance schematic for the central station, showing a breakdown of heat leakage through the various components of the central station during the prototype test.
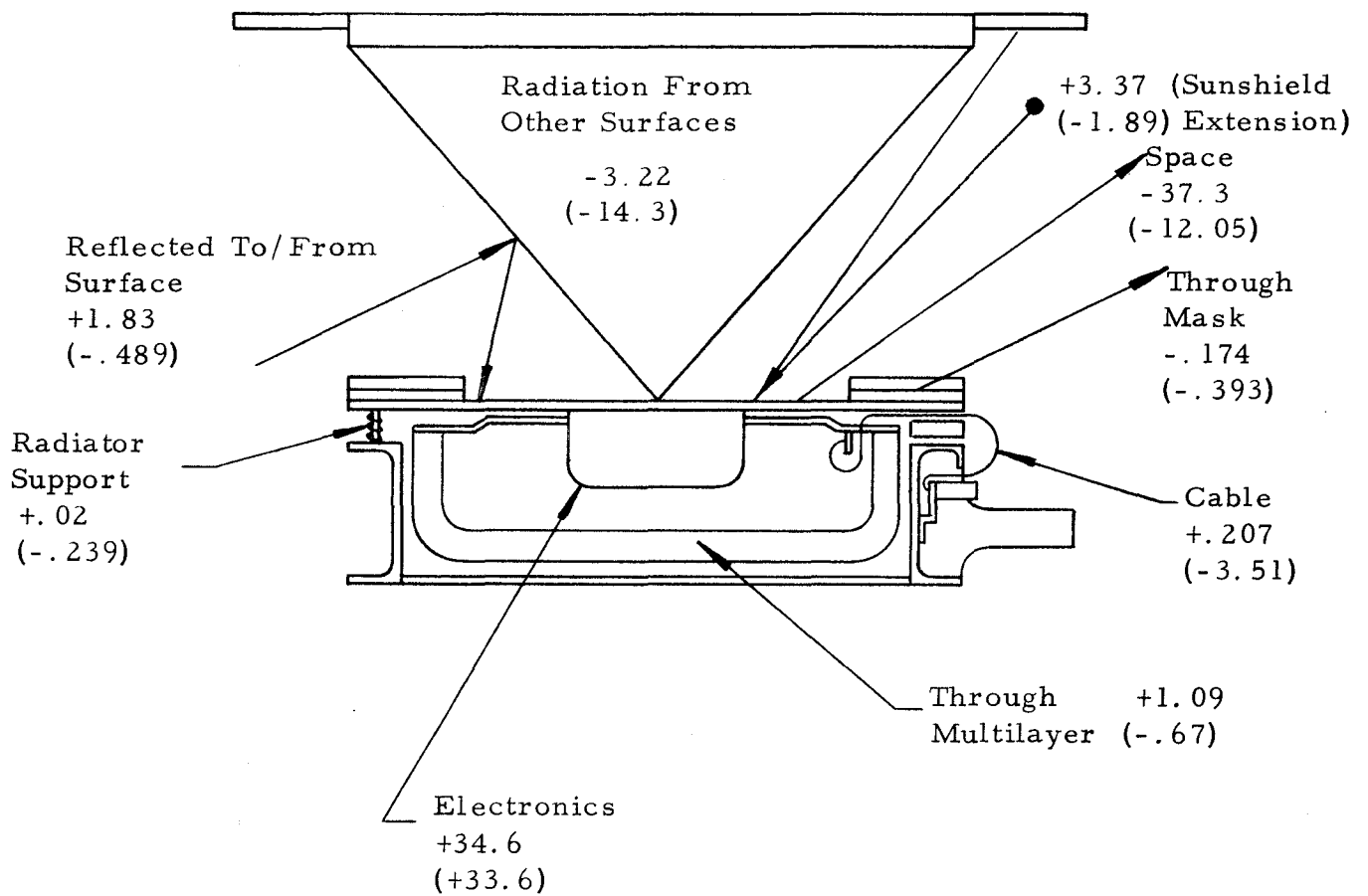
3.3.1 Lunar Noon

Referring to Table 8 and examining first the radiator plate results it may be determined that measured and predicted values of average noon radiator temperature are 105°F and 121°F respectively. This difference of 16°F represents a deviation of predicted from measured results of less than 3%. Considering individual points on the radiator, the maximum deviation is found to be approximately 3.5%. Agreement on the sunshield is very good with a maximum variation of 6°F or approximately 1.2%. The variation between measured and predicted temperatures on the primary structure ranged from 25°F to 46°F. The higher temperature observed on the primary structure are attributed to the heat dissipation of the extended resistor network mounted on the primary structure, and the associated temperature gradients.

3.3.2 Lunar Night

Drawing comparisons in the same manner as for lunar noon, the measured and predicted values of average radiator temperature are -15°F and -10°F respectively, a deviation of 5°F or approximately 1%. It might be expected that agreement would be better here since the total lunar night thermal environment is relatively uniform and hence thermal interplay among various parts of the system is relatively less important. There is some variation between predicted and measured values of the primary structure temperatures which is again explained by the external resistor dissipation. The difference between measured and predicted sunshield temperatures is explained by higher than anticipated conduction between sunshield and primary structure through the extenders.

4.0 Conclusions

Several significant conclusions may be drawn from the central station Prototype "A" test results, the associated analytical predictions and correlation.

Radiation From
Other Surfaces

-3.22
(-14.3)

+3.37 (Sunshield
(-1.89) Extension)

Space
-37.3
(-12.05)

Reflected To/From
Surface
+1.83
(-.489)

Through
Mask
-.174
(-.393)

Radiator
Support
+.02
(-.239)

Cable
+.207
(-3.51)

Through   +1.09
Multilayer   (-.67)

Electronics
+34.6
(+33.6)

+   Into Radiator
-   From Radiator   (Watts)

xxx   Noon
(xxx)   Night

Figure 15 ALSEP Proto "A" Central Station Heat
Balance for Lunar Noon and Lunar Night

1. The central station thermal performance was satisfactory and perhaps slightly better than expected. A lunar noon to lunar night radiator temperature swing of $+121^\circ F$ to $-10^\circ F$ was predicted whereas a range of $+105^\circ F$ to $-15^\circ F$ was realized.

2. The usefulness of the analytical model (described in this report) as a tool in predicting central station thermal performance was demonstrated. The variation between measured and predicted radiator temperature was less than 3%.

3. The objective of isolation of the Central Station radiator plate from the lunar environment was satisfactorily achieved. The successful thermal isolation is directly reflected in the test results, and the analytical model. The analytical and test results show that significant variation of the sunshield and/or primary structure temperatures has little or no effect on the overall radiator performance.

APPENDIX *

RADIOSITY METHOD FOR RADIANT
INTERCHANGE CALCULATIONS

Consider a surface, i, which has a total heat flux, H_i, impinging upon it and a total heat flux, J_i, leaving it. The quantity J_i will be termed "radiosity".

H_i J_i

i
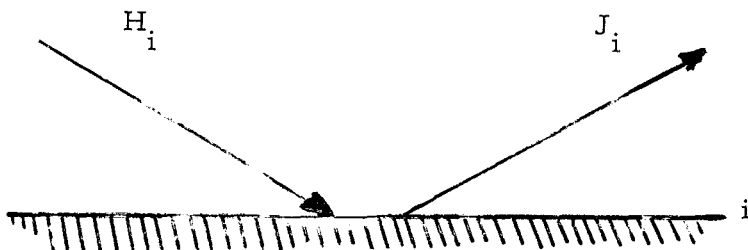
NOTE: Throughout this discussion, the term total heat flux is used to signify all of the heat flux traveling in a specified path and direction, while net heat flux is the difference between the total heat flux entering and that leaving a surface.

The net heat rate leaving surface i is then:

$$\dot{q}_{NET_i} = A_i (J_i - H_i) \tag{1}$$

where A_i = area of surface i

For any surface:

$$\alpha + \rho + \tau = 1 \text{ (first law)}$$

where:

α = absorptance of the surface

ρ = reflectance of the surface

τ = transmittance of the surface

---

* Abstracted from Bendix Report BSR-2021, "Advanced Analytical Techniques for Thermal Control."

assume that for surface i:

$$\tau_i = 0 \text{ (opaque surface)}$$

then:

$$\alpha_i + \rho_i = 1$$

assume in addition that:

$$\alpha_i = \epsilon_i \text{ (gray body)} \tag{2}$$

then:

$$\epsilon_i + \rho_i = 1 \tag{3}$$

Now the <u>total heat flux</u>, J_i, leaving surface i consists of both emitted and reflected radiation. By the definition of emissivity and reflectivity, we can conclude that:

$$J_i = E_{b_i} \epsilon_i + \rho_i H_i \tag{4}$$

where E_{b_i} = emissive power of a black body at the temperature of surface i.

Combining equations 3 and 4, we have:

$$J_i = E_{b_i} \epsilon_i + (1 - \epsilon_i) H_i$$

or,

$$H_i = \frac{J_i - E_{b_i} \epsilon_i}{(1 - \epsilon_i)} \tag{5}$$

Combining equations 1 and 5, we get:

$$q_{NET_i} = A_i \left[J_i - \frac{(J_i - E_{b_i} \epsilon_i)}{(1 - \epsilon_i)} \right]$$

$$= \frac{A_i \epsilon_i}{(1 - \epsilon_i)} (E_{b_i} - J_i) \qquad (6)$$

The significance of equation 6 is that it expresses the net heat rate leaving surface i as a function only of its emissivity, ϵ_i, area, A_i, and the difference between its black body potential, E_{b_i}, and its radiosity, J_i.

In this way, the net heat rate leaving surface i is expressed independently of the total heat rate, H_i, entering it.

Consider now the case of radiant interchange between surface i and another surface, j.

The total heat rate leaving surface i is simply:

$$A_i J_i$$

Of this amount, the fraction

$$A_i J_i F_{ij}$$

impinges directly upon surface j, where F_{ij} is the geometric view factor from surface it to surface j.

Similarly, the total heat rate leaving surface j is:

$$A_j J_j$$

and the fraction:

$$A_j J_j F_{ji}$$

47

of this quantity impinges directly upon surface i.

The net heat rate from surface i to surface j is simply the difference between the heat rate leaving i and impinging upon j, and that leaving j and impinging upon i.

Then,

$$\dot{q}_{NET_{i_j}} = A_i J_i F_{ij} - A_j J_j F_{ji} \tag{7}$$
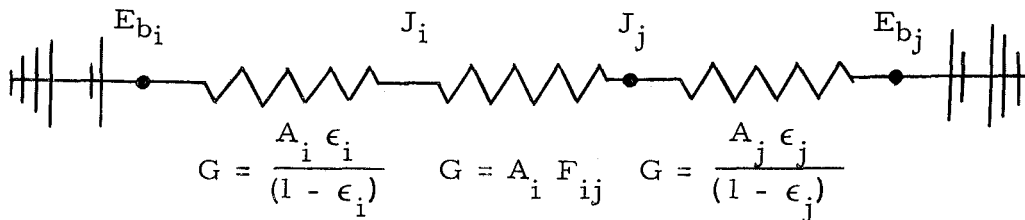
By the reciprocity theorem,

$$A_i F_{ij} = A_j F_{ji} \tag{8}$$

Combining equations 7 and 8, we get:

$$\dot{q}_{NET_{i_j}} = A_i F_{ij} (J_i - J_j) \tag{9}$$

Equation 9 suggests that the net heat rate from surface i to surface j can be expressed as the product of a constant $(A_i F_{ij})$ and the difference of the radiosities of surfaces i and j. Equation 6, on the other hand, indicates that the net heat rate leaving surface i is the product of a constant $\dfrac{A_i \epsilon_i}{1 - \epsilon_i}$ and the difference between its black body potential E_{b_i}, and its radiosity, J_i.

From the above, one can construct an analogous resistance-type electrical network in which voltage is equivalent to emissive power and current to heat rate. The equivalent network for the two-surface radiant interchange problem described above would appear as follows:

$$E_{b_i} \qquad J_i \qquad J_j \qquad E_{b_j}$$

$$G = \frac{A_i \epsilon_i}{(1 - \epsilon_i)} \qquad G = A_i F_{ij} \qquad G = \frac{A_j \epsilon_j}{(1 - \epsilon_j)}$$

In this analogous network, one can see that the radiosities J_i and J_j act as floating potentials having values intermediate between E_{b_i} and E_{b_j}. From this analogy it is also clear that, if the emissivity of surface i were equal to 1.0, the value of the leftmost conductor would be infinity. As a result, the value of J_i would be identical to E_{b_i}. In physical terms, this means that all of the heat leaving a black body is due to emittance, and none to reflectance.

The analogy developed above for two nodes can be extended to any number of nodes by treating each pair of nodes having non-zero geometric view factors to each other in the same way as surfaces i and j were treated above. For example, the addition of two nodes k and l to the system would result in the following network:
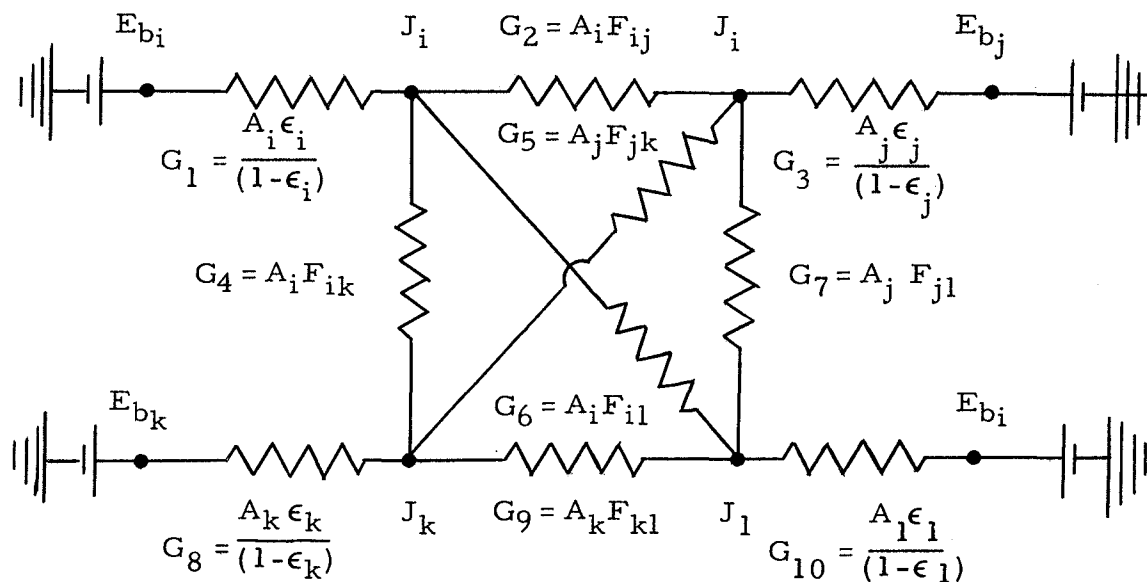
Such an extension is valid because the construction of the equivalent network for radiant interchange between two surfaces requires no assumptions regarding the existence of possible additional surfaces in the system (see derivations for equations 6 and 9 above).

If more than two surfaces are present, the total radiant heat interchange between any two surfaces can consist of one direct component and a number of indirect components. These indirect components are a result of reflection and reradiation via other surfaces in the system. As an example, the direct radiation from i to j in the four-surface network illustrated above flows through conductor No. 2, while the indirect components can flow through conductors 4, 5, 6, 7, and 9.

REFERENCES

1. Oppenheim, A. K., "Radiation Analysis by the Network Method", American Society of Mechanical Engineers, Transactions, Vol. 78, No. 4 (May 1956), pp. 725-735.

2. Ziering, M. B. and Sarofin, A. F., "The Electrical Network Analog to Radiactive Transfer: Allowance for Specular Reflection", American Society of Mechanical Engineers, Transactions, Journal of Heat Transfer, August 1966, pp. 341-342.

3. Ziering, M. B. and Sarofin, A. F. and Raymond, R. J., "Computer Programs for the Computation of Radiant Exchange in Specular-Diffuse Enclosures"; The Dynatech Corporation, 17 Tudor Street Cambridge, Massachusetts 02139; Dynatech Report No. 607, Dynatech Project No. NAS-11.

4. Toups, K. A., "A General Computer Program for the Determination of Radiant-Interchange Configuration and Form Factors - CONFAC II", North American Aviation, Inc., Space and Information Systems Division, Report No. SID 65-1043-2, October 1965.

5. Brown, A. I., and Marco, S. M., "Introduction to Heat Transfer," McGraw-Hill Book Company, New York, 1942.

6. Bendix Thermal Analyzer Computer Program

7. ALSEP System Thermal Test Procedure No. 2333040-B, 1 December 1967.